jmb Article

Ligand Binding Reduces Conformational Flexibility in the Active Site of Tyrosine Phosphatase Related to Biofilm Formation A (TpbA) from *Pseudomonas aeruginosa*

Dorothy Koveal[1], Michael W. Clarkson[2], Thomas K. Wood[3], Rebecca Page[1] and Wolfgang Peti[2,4]

1 - Department of Molecular Biology, *Cell Biology and Biochemistry, Brown University, Providence, RI 02903, USA*
2 - Department of Molecular Pharmacology, *Physiology and Biotechnology, Brown University, Providence, RI 02903, USA*
3 - Department of Chemical Engineering, *Pennsylvania State University, University Park, PA 16802-4400, USA*
4 - Department of Chemistry, *Brown University, Providence, RI 02903, USA*

Correspondence to Rebecca Page and Wolfgang Peti: *Rebecca_Page@brown.edu; Wolfgang_Peti@brown.edu*
http://dx.doi.org/10.1016/j.jmb.2013.03.023
Edited by R. Kriwacki

Abstract

Tyrosine phosphatase related to biofilm formation A (TpbA) is a periplasmic dual-specificity phosphatase (DUSP) that controls biofilm formation in the pathogenic bacterium *Pseudomonas aeruginosa*. While DUSPs are known to regulate important cellular functions in both prokaryotes and eukaryotes, very few structures of bacterial DUSPs are available. Here, we present the solution structure of TpbA in the ligand-free open conformation, along with an analysis of the structural and dynamic changes that accompany ligand/phosphate binding. While TpbA adopts a typical DUSP fold, it also possesses distinct structural features that distinguish it from eukaryotic DUSPs. These include additional secondary structural elements, β0 and α6, and unique conformations of the variable insert, the α4–α5 loop and helix α5 that impart TpbA with a flat active-site surface. In the absence of ligand, the protein tyrosine phosphatase loop is disordered and the general acid loop adopts an open conformation, placing the catalytic aspartate, Asp105, more than 11 Å away from the active site. Furthermore, the loops surrounding the active site experience motions on multiple timescales, consistent with a combination of conformational heterogeneity and fast (picosecond to nanosecond) timescale dynamics, which are significantly reduced upon ligand binding. Taken together, these data structurally distinguish TpbA and possibly other bacterial DUSPs from eukaryotic DUSPs and provide a rich picture of active-site dynamics in the ligand-free state that are lost upon ligand binding.

Introduction

The dual-specificity phosphatases (DUSPs) are cysteine-based phosphatases that catalyze the dephosphorylation of substrates on phosphorylated tyrosine, serine, and threonine residues. As a subset of the protein tyrosine phosphatase (PTP) superfamily, DUSPs contain the highly conserved signature motif HCXXXXXR and a conserved aspartic acid residue that is important for catalysis.[1] Eukaryotic DUSPs play critical regulatory roles in numerous cellular processes including proliferation, apoptosis, differentiation, and stress response.[2–4] In bacteria, DUSPs are intimately involved in mechanisms controlling pathogenicity, including manipulation of host cell proteins[5] and polysaccharide production, which is crucial for biofilm growth.[6] Importantly, outside of the conserved signature motif, there is low sequence homology between bacterial and eukaryotic DUSPs. Thus, despite the wealth of information available for eukaryotic DUSPs, little is known about the structural features specific to bacterial DUSPs.

Tyrosine phosphatase related to biofilm formation A (TpbA) is a DUSP from the pathogenic bacterium *Pseudomonas aeruginosa*. Infection by *P. aeruginosa* is one of the most common and life-threatening diseases faced by patients suffering from cystic fibrosis.[7] The persistence of *P. aeruginosa* infections

is linked to its ability to form biofilms, organized communities of microorganisms encased in a polymeric matrix.[8] Critically, TpbA reduces biofilm formation in response to acyl homoserine lactone, a quorum-sensing molecule.[6] TpbA is targeted to the periplasm and is a negative regulator of TpbB/YfiN, a diguanylate cyclase (GGDEF). TpbB catalyzes the synthesis of 3,5-cyclic diguanylic acid, an important second messenger that increases transcription across the *pel* operon, which, in turn, leads to the formation of pellicles, one of the major biofilms in *P. aeruginosa*. By attenuating the activity of TpbB through dephosphorylation of both tyrosine and serine/threonine residues, TpbA reduces the intracellular concentration of 3,5-cyclic diguanylic acid, which leads to a reduction in biofilm formation.[9] The essential role of TpbA in regulating *P. aeruginosa* biofilm formation makes it a potential drug target for *P. aeruginosa* infections.

PTPs, LMW-PTPs, and DUSPs, such as TpbA, share a common catalytic mechanism.[10] However, apart from the loops that define the active site, they have very low sequence homology. The active site is defined by the PTP-loop, which includes the conserved cysteine that functions as a catalytic nucleophile, and the general acid loop, which contains the catalytic aspartic acid that functions as an acid/base during the dephosphorylation reaction. In PTPs, substrate binding is accompanied by rotation of the general acid loop, resulting in a movement of the catalytic acid/base by up to 10 Å.[11] This converts the PTP active site from an open, catalytically inactive state to a "closed," catalytically active state. In contrast, far less is known about the changes that occur in DUSPs during the catalytic cycle, especially DUSPs from bacteria. This is because only a handful of DUSPs have been studied in the open conformation and even less using nuclear magnetic resonance (NMR) spectroscopy. Thus, very little is known about the dynamics of the loops that define the active site between the ligand-free and ligand-bound states and the role of loop dynamics in ligand binding and catalysis.

Here, we report the solution NMR structure of TpbA, the first structure of a bacterial periplasmic DUSP. We show that TpbA adopts a canonical DUSP fold, similar to eukaryotic DUSPs. However, TpbA also has a number of structural features that distinguish it from its eukaryotic counterparts, including additional secondary structural elements and distinct loop conformations. In addition, because the structure of TpbA was determined in the ligand-free state, it is in an open conformation, with an open general acid loop and a disordered PTP loop. Most importantly, we performed ligand titrations using inorganic phosphate to identify all residues of TpbA that respond to ligand binding, which include the PTP loop, the general acid loop, and the α4–α5 loop. Finally, we provide the first detailed description of changes in the motions of these functionally important loops in both the absence and presence of ligand, revealing that ligand binding "locks" out conformational dynamics that occur on multiple timescales in loops surrounding the active site.

Results

The first structure of a bacterial periplasmic DUSP, TpbA

TpbA (residues 29–218, 21 kDa) showed high levels of soluble overexpression in *Escherichia coli* and behaves as a monomer in solution as verified by size-exclusion chromatography. It can be concentrated to 1 mM without precipitation or signs of aggregation and yields a high-quality two-dimensional (2D) [^{1}H,^{15}N] heteronuclear single quantum coherence (HSQC) spectrum. Out of 183 expected non-proline amide backbone cross-peaks, 164 could be assigned with high confidence.[12] To overcome the lack of nuclear Overhauser enhancement (NOE)

Table 1. NMR refinement statistics for ligand-free TpbA

	Protein
NMR distance and dihedral constraints	
Distance constraints	
Total NOE	2504
Intra-residue	581
Inter-residue	
Sequential ($\|i-j\|=1$)	701
Medium range ($\|i-j\|<4$)	515
Long range ($\|i-j\|>5$)	707
Intermolecular	0
Hydrogen bonds	0
Total dihedral angle restraints	270
φ	135
ψ	135
Structure statistics	
Violations (mean and SD)	
Distance constraints (Å)	0.0175 ± 0.0010
Dihedral angle constraints (°)	0.481 ± 0.044
Maximum dihedral angle violation (°)	3.658 ± 0.709
Maximum distance constraint violation (Å)	0.226 ± 0.041
Deviations from idealized geometry	
Bond lengths (Å)	0.0106 ± 0.0002
Bond angles (°)	1.26 ± 0.03
Impropers (°)	1.46 ± 0.06
Average pairwise r.m.s.d.[a] (Å)	
Heavy	7.85 ± 2.86
Backbone	7.56 ± 2.85
Secondary structure heavy[b]	1.02 ± 0.09
Secondary structure backbone[b]	0.56 ± 0.08

[a] Pairwise r.m.s.d. was calculated among 20 refined structures using MOLMOL.

[b] Pairwise r.m.s.d. was calculated among secondary-structure residues only, excluding helix α6 (residues 40–44, 49–51, 56–59, 64–73, 77–79, 87–90, 96–98, 109–122, 128–131, 136–149, 155–164, and 175–182).

distance constraints in areas with unassigned amide backbone NH pairs, we assigned all non-exchangeable side-chain hydrogen atoms using different HCCH-based and three-dimensional (3D) ^{13}C-resolved [^{1}H,^{1}H] NOE spectroscopy (NOESY) experiments. A total of 2504 NOE-based distance restraints and 270 dihedral angle restraints were used for the 3D structure calculation of TpbA$_{29–218}$. The 20 conformers from the final CYANA cycle with the lowest residual CYANA target function values were energy minimized in a water shell[13,14] (Table 1). The core of TpbA, which is composed of residues 40–194, is well defined and adopts a compact fold. It consists of a central six-stranded β-sheet with a folding topology +1, +1, +2*x*, +1*x*, −2*x*, flanked by five α-helices on one side and two α-helices on the other (Fig. 1a). Residues 29–39 and 195–218 are flexible and unstructured in solution based on chemical shift index calculations derived from C$^{\alpha}$ and C$^{\beta}$ chemical shifts and ^{15}N [^{1}H] NOE analysis[12] (Supplementary Fig. 5c). As a result, these regions lack NOE-based distance restraints (Supplementary Fig. 1a) and are poorly defined in the final structural bundle of TpbA (Supplementary Fig. 1b).

TpbA adopts a eukaryotic-like DUSP fold, confirming bioinformatics predictions and previous experiments showing phosphatase activity against phosphotyrosine (pTyr), phosphoserine (pSer), and phosphothreonine (pThr).[6,9] The active-site architecture of the DUSP catalytic domain is defined by four loops (Fig. 1b): (1) the PTP loop, which contains the conserved cysteine that functions as the catalytic nucleophile; (2) the general acid loop, which contains a conserved aspartic acid residue that functions as a catalytic acid/base; (3) the variable insert, which varies in sequence and length among DUSPs and may be involved in substrate recognition; and (4) loop α4–α5, which is in the position of the Q-loop in PTPs. Also, DUSPs have a characteristically shallow active site (~6 Å) that allows access of both pTyr and pSer/pThr to the active-site

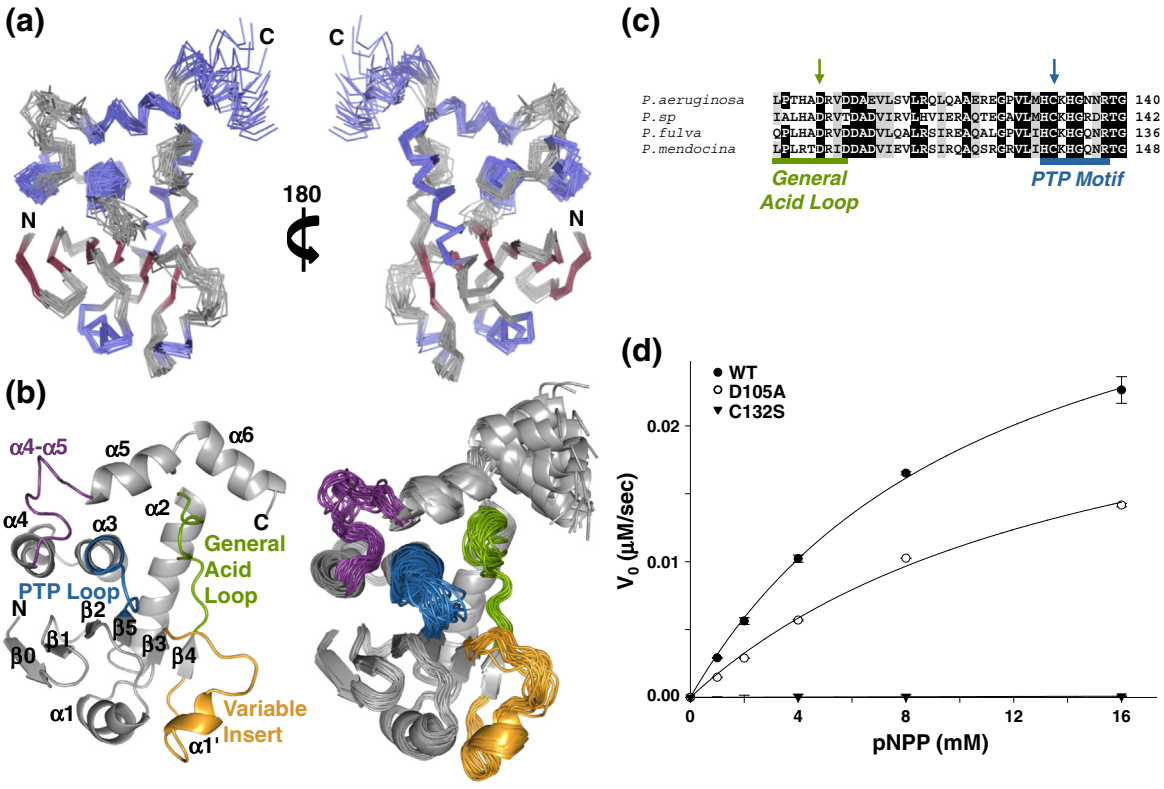

Fig. 1. TpbA adopts a canonical DUSP fold. (a) Bundle of the 20 lowest-energy structures of TpbA. The superposition is the best fit of the structured regions, excluding helix α6, which are colored blue for α-helices and red for β-strands. (b) *Left*, The lowest-energy structure of TpbA is shown as a cartoon, with functionally important regions highlighted, including the PTP loop (blue), the general acid loop (green), the variable insert (yellow), and the α4–α5 loop (purple). *Right*, Bundle in (a) shown as a cartoon using the same color scheme as in (b). (c) Sequence conservation of the general acid loop and PTP motif across bacterial species. Identical residues are highlighted black, while similar residues are highlighted gray. The catalytic residues, C132 and D105, are marked with blue and green arrows, respectively. (d) Dephosphorylation of *p*NPP by WT (•), D105A (○), and C132S (▾) TpbA mutants.

cysteine, whereas the deeper active site in specific PTPs (~9 Å) is selective for pTyr. As expected for a DUSP, TpbA has a shallow active site, consistent with its ability to dephosphorylate pTyr, pSer, and pThr residues. While the structures of numerous eukaryotic DUSPs are available, TpbA is only the fourth DUSP from bacteria whose structure has been determined.[15–17] Most importantly, this is the first structure of a bacterial DUSP solved in a ligand-free state, which adopts an open general acid and disordered PTP loop, giving valuable insights into the active-site architecture in the absence of ligand as well as the molecular basis for substrate binding.

Cys132 and Asp105 mediate catalysis in TpbA

The consensus catalytic sequence that defines Type 1 cysteine-based PTPs, which includes DUSPs, is HCXXXXXR.[1] In TpbA, this sequence is ^{131}HCKHGNNR^{138}, with Cys132 predicted to function as the catalytic nucleophile during catalysis (Fig. 1c). Although three Asp residues are present in the general acid loop, only Asp105 and Asp108 are conserved among multiple *Pseudomonas* species. Furthermore, our structure suggests that only Asp105 is capable of accessing the active site without requiring large, global structural rearrangements.

To test the role of Asp105 and Cys132 in catalysis, we measured the catalytic activity of wild-type (WT) TpbA, a D105A mutant, and a C132S mutant against the general PTP and DUSP model substrate, *p*-nitrophenyl phosphate (*p*NPP; Fig. 1d). The Cys-to-Ser mutation is a well-characterized mutation that typically results in a complete loss of catalytic activity in PTPs and DUSPs.[18–21] Mutation of the conserved Asp also leads to a loss of catalytic activity, although a subset of DUSPs/PTPs are only mildly affected.[17,22–24] We found that while WT TpbA effectively dephosphorylated *p*NPP, the C132S mutant had no detectable activity, and the D105A mutant resulted in a 53% decrease in catalytic efficiency (Table 2). These data, in combination with the structure, support the role of Asp105 as the general acid/base and Cys132 as the catalytic cysteine in the TpbA-catalyzed dephosphorylation reaction.

TpbA is unique among DUSPs

A search for homologous structures using the DALI server identified DUSP23,[25] a eukaryotic atypical DUSP, as the structure most similar to TpbA, with a DALI *Z*-score of 10.1. The next most similar structures are DUF442, a bacterial protein predicted to be a DUSP from *Shewanella putrefaciens* (*Z*-score = 9.5); CDC14B2,[26] a eukaryotic DUSP in the PTEN family (*Z*-score = 9.5); and SEX4,[27] a DUSP from *Arabidopsis thaliana* (*Z*-score = 9.4).

A comparison of TpbA with these and other DUSP structures reveals that, while TpbA adopts a canonical DUSP architecture, it is also unique (Fig. 2a). First, compared with other DUSPs, TpbA has an additional helix, helix α6. This helix does not make any stable contacts with the rest of the phosphatase domain and no NOEs are observed between it and the remainder of the protein. However, helix α6 is required for TpbA solubility, as deletion of this helix results in insoluble expression of TpbA in *E. coli*. Second, most DUSPs have five β-strands that form the central β-sheet. In contrast, the central β-sheet of TpbA is composed of six β-strands (Fig. 2b). The only other DUSPs that have a six-stranded central β-sheet are DUSP6 (PYST/MKP3) and DUSP9 (MKP4). However, in these DUSPs, the additional strand is located in the variable insert (Fig. 2c). In contrast, the additional β-strand in TpbA is located at the N-terminus of the protein, capping the β-sheet, a feature that, to our knowledge, is unique to TpbA.

Not only does TpbA possess additional secondary structural features, but other conserved regions of the protein adopt conformations distinct from other DUSPs. First, in some DUSPs, a residue in the variable insert makes polar contacts with the conserved Arg in the PTP motif, positioning the Arg side chain in the active site. In TpbA, the orientation of the variable insert is disengaged from the active site, leaving the active-site face of TpbA flat and open. This is significant because the variable insert contributes to the depth of the active site.[27] Second, the conformation of the α4–α5 loop and helix α5 is unique to TpbA. In most DUSPs, this loop defines the upper boundary of the PTP pocket (see, for example, DUSP23, CDC14B2, and SEX4 in Fig. 2a), and in human DUSPs, this loop is also conserved in sequence (known as the R-motif[28]). In contrast, in TpbA, this loop folds away from the PTP loop, adopting a conformation more similar to that of another bacterial DUSP, DUF442. Finally, the AYLM motif, which forms part of the extended signature

Table 2. Enzymatic activity of WT and TpbA variants

	V_{max} (μM min^{-1})	k_{cat} (s^{-1})	K_m (mM)	k_{cat}/K_m (M^{-1} s^{-1})	Fold difference in k_{cat}/K_m
WT	1.55 ± 0.05	1.62×10^{-3}	11.21 ± 0.72	0.14	1.00
D105A	1.12 ± 0.11	1.17×10^{-3}	15.22 ± 2.62	0.08	0.53
C132S	ND	ND	ND	NA	NA

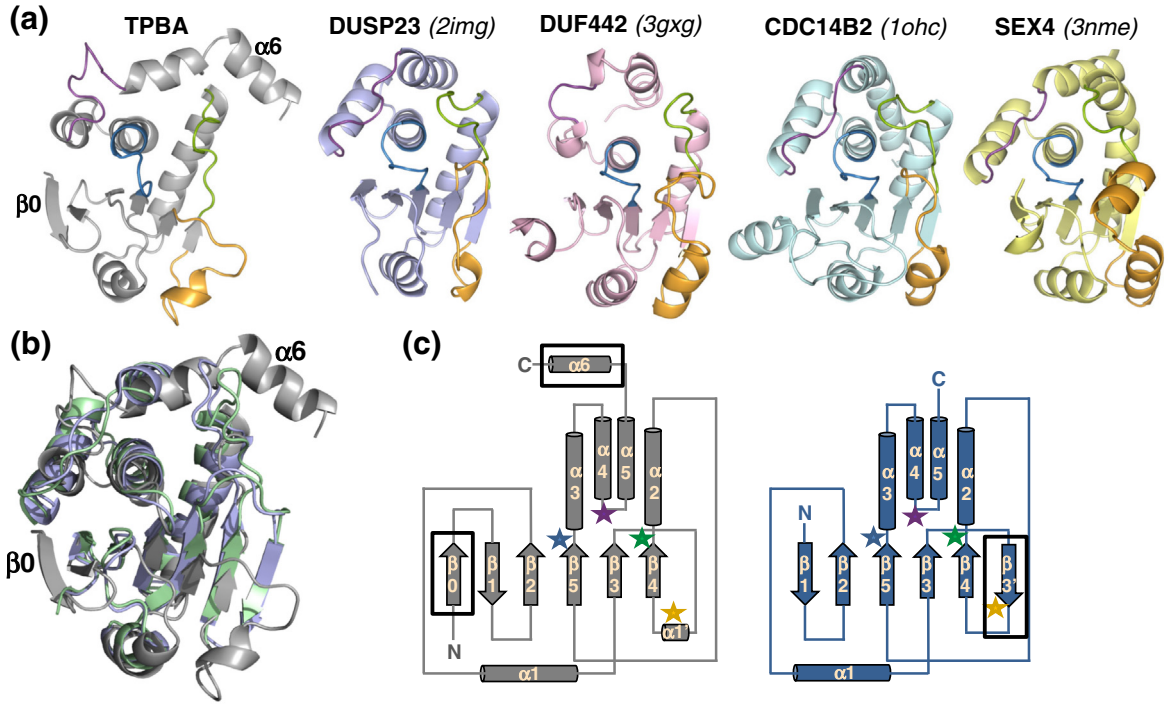

Fig. 2. TpbA is unique among DUSPs. (a) TpbA and its four closest structural homologs, DUSP23 (PDB ID 2IMG; *Z*-score = 10.1, light purple), DUF442 (PDB ID 3GXG, *Z*-score = 9.5, pink), CDC14B2 (PDB ID 1OHC, *Z*-score = 9.5, light cyan), and SEX4 (PDB ID 3NME, *Z*-score = 9.4, yellow); the coloring scheme of loops is the same as in Fig. 1b. (b) Overlay of TpbA with DUSP6 (blue, PYST/MKP3) and DUSP9 (green, MKP4). Structural features unique to TpbA, strand β0 and helix α6, are labeled. (c) Cartoon illustrating the secondary-structure topology of TpbA (gray) and DUSP6/DUSP9 (blue). The additional secondary structural elements in these DUSPs compared to canonical DUSPs are boxed. Colored stars indicate the locations of the loops colored in (a).

sequence of the DUSP family,[28] is also not conserved in TpbA. This motif has been replaced by the sequence MYRIV in helix α3, resulting in an alternate orientation of helix α5 that allows it to bridge helix α2 and helix α3. This in turn enables helix α6 to point away from the catalytic domain, a conformation unique to TpbA.

Stabilization of the TpbA active site upon ligand binding

In the ligand-free form of TpbA, the majority of the unassigned amide backbone NH pairs (Ser80, Phe81, Ile82, Lys83, Ala104, Glu118, Lys133, His134, Gly135, Asn136, Thr139, Gly140, Phe142, Ala158, Asp172, Met173, Arg174, Leu204, and His206) belong to the variable insert, the PTP loop, and the α4–α5 loop. Due to the lack of NOE distance constraints, these loops do not converge as well as the rest of the core phosphatase domain. In TpbA, there are, on average, 35 NOE-derived distance restraints per residue for all well-defined regions of the structure, whereas there are only 17 restraints per residue in the loop regions mentioned above (Supplementary Fig. 1a). This lack of convergence in loop conformations has also been observed for other phosphatases, including the DUSP PRL-3,[29] a bacterial acylphosphatase,[30] and DUSP PAC-1.[31]

To determine whether the conformation of the active site is stabilized upon ligand binding, we performed titration experiments of TpbA with sodium phosphate using protein:phosphate ratios ranging from 1:10 to 1:320, the latter of which resulted in full saturation (Fig. 3; Supplementary Fig. 2). The number of NH cross-peaks in a 2D [^{1}H,^{15}N] HSQC spectrum of TpbA increases from 164 in the ligand-free state to 172 in the phosphate-bound state. The increased number of NH cross-peaks indicates that these residues undergo a significant change in their backbone dynamics from the intermediate-timescale to the fast-timescale exchange regime. Indeed, inspection of the 2D [^{1}H,^{15}N] HSQC spectra reveals increases in peak intensities for residues in the general acid loop, the PTP motif, helix α3, and the α4–α5 loop in phosphate-bound *versus* ligand-free TpbA, consistent with a shift from the intermediate- to the fast-exchange regime (Fig. 3a; Supplementary Fig. 2). Asp105 experiences the greatest relative change in intensity, as it is 6.7 times more intense in the phosphate-bound TpbA 2D [^{1}H,^{15}N] HSQC

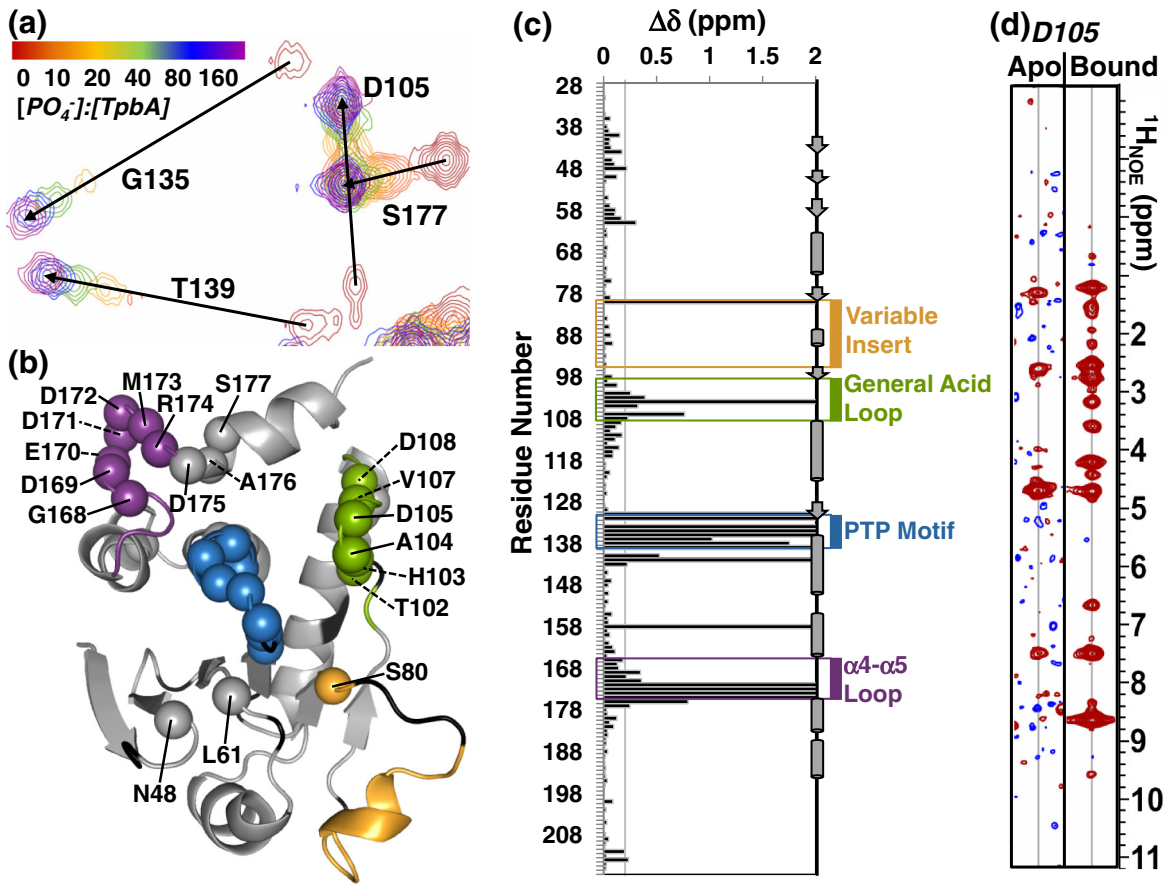

Fig. 3. Phosphate binding involves the general acid loop, the PTP, and the α4–α5 loops. (a) Portion of the 2D [^{1}H, ^{15}N] HSQC spectrum of ^{15}N-TpbA from increasing titrations of sodium phosphate. CSPs (indicated by arrows) and intensity changes are observed for residues surrounding the active site, including G135 and T139 in the PTP loop and D105 in the general acid loop. (b) Residues with CSP $\geq$ 0.2 ppm are mapped onto the structure of TpbA and shown as spheres using the same color scheme as in Fig. 1b. (c) Histogram showing the CSPs between ligand-free and phosphate-bound TpbA. ^{15}NH resonances that are only assigned in either ligand-free or phosphate-bound TpbA are set to an arbitrary value of 2 ppm. Functionally important loops are boxed, labeled, and colored as in Fig. 1b. (d) The ^{1}H NOESY pattern of D105 changes upon phosphate binding. Strips corresponding to the D105 backbone H_N spin system of ligand-free (*left*) and phosphate-bound TpbA (*right*). In ligand-free TpbA, only intra-residue NOEs are observed. Upon phosphate binding, 11 new inter-residue NOEs appear, consistent with D105 closing over the TpbA active site upon ligand binding.

spectrum than in the ligand-free TpbA spectrum. Additionally, Gly135 and Thr139 in the PTP motif and Asp171 and Ala176 in the α4–α5 loop all have 3 to 3.5 times greater intensity in the phosphate-bound 2D [^{1}H, ^{15}N] HSQC spectrum. Other residues in these regions (His103, Asn136, Phe142, and Asp172) are broadened beyond detection in the 2D [^{1}H, ^{15}N] HSQC spectrum of ligand-free TpbA but show average cross-peak intensities in the phosphate-bound 2D [^{1}H, ^{15}N] HSQC TpbA spectrum. Interestingly, this behavior is distinct from that observed for the low-molecular-weight tyrosine phosphatase MptpA, where many more NH cross-peaks become broadened in the phosphate-bound form in the PTP-loop and those amino acids flanking the D- and W-loops.[32]

To better understand these changes, we performed the sequence-specific backbone assignment of TpbA in the phosphate-bound state. Chemical shift index values show that the secondary-structure elements are identical in ligand-free and phosphate-bound TpbA (Supplementary Fig. 3). Chemical shift perturbation (CSP) mapping of ligand-free and phosphate-bound TpbA shows that the PTP, the general acid, and the α4–α5 loops are most affected by phosphate binding (Fig. 3b and c). Interestingly, the variable insert is not affected, except for a single residue, S80. This differs from the human DUSP PRL-3 where all variable insert residues have CSPs upon phosphate binding.[29]

We also measured a 3D ^{15}N-resolved [^{1}H, ^{1}H] NOESY spectrum of phosphate-bound TpbA.

Changes in NOEs of loop residues, particularly D105, are consistent with a conformational change in which the general acid loop is closed over the TpbA active site (Fig. 3d; Supplementary Fig. 4). Additionally, the side-chain NH_2 group of N48 in the β1–β2 loop experiences large CSPs and dramatic change of NOEs upon phosphate binding (Fig. 4). In the crystal structure of DUSP23, which has a closed general acid loop, residue N7 in the β1–β2 loop makes polar contacts with the backbone carbonyls of L97 and G98 in the PTP loop (Fig. 4a). If the PTP loop of TpbA adopted a conformation similar to DUSP23, NOEs between N48 $H^{\delta21}/H^{\delta22}$ and the PTP loop should be observed. However, the structure of open conformation TpbA shows that N48 is 11 Å away from H134 and G135 in the PTP loop (Fig. 4b). Yet, N48 is clearly affected by ligand binding as the NH_2 side-chain protons experience large CSPs in response to phosphate binding (Fig. 4c). Thus, while no NOEs are detected in the ligand-free open conformation (Fig. 4d), in the phosphate-bound state, N48 $H^{\delta21}/H^{\delta22}$ protons have many medium-range NOEs with H134 $H^{\beta2}/H^{\beta3}$ and N136 Qβ, consistent with the conformation of the PTP motif observed in the closed structure of DUSP23 (Fig. 4e). Taken together, these data show that phosphate-bound TpbA adopts the expected active-site architecture observed in numerous structures of DUSPs in the closed conformation.[25,33–35]

Dynamics of ligand-free and phosphate-bound TpbA

To better understand the dynamics changes that occur upon ligand binding in TpbA, we performed ^{15}N-based auto-correlated relaxation analysis of the

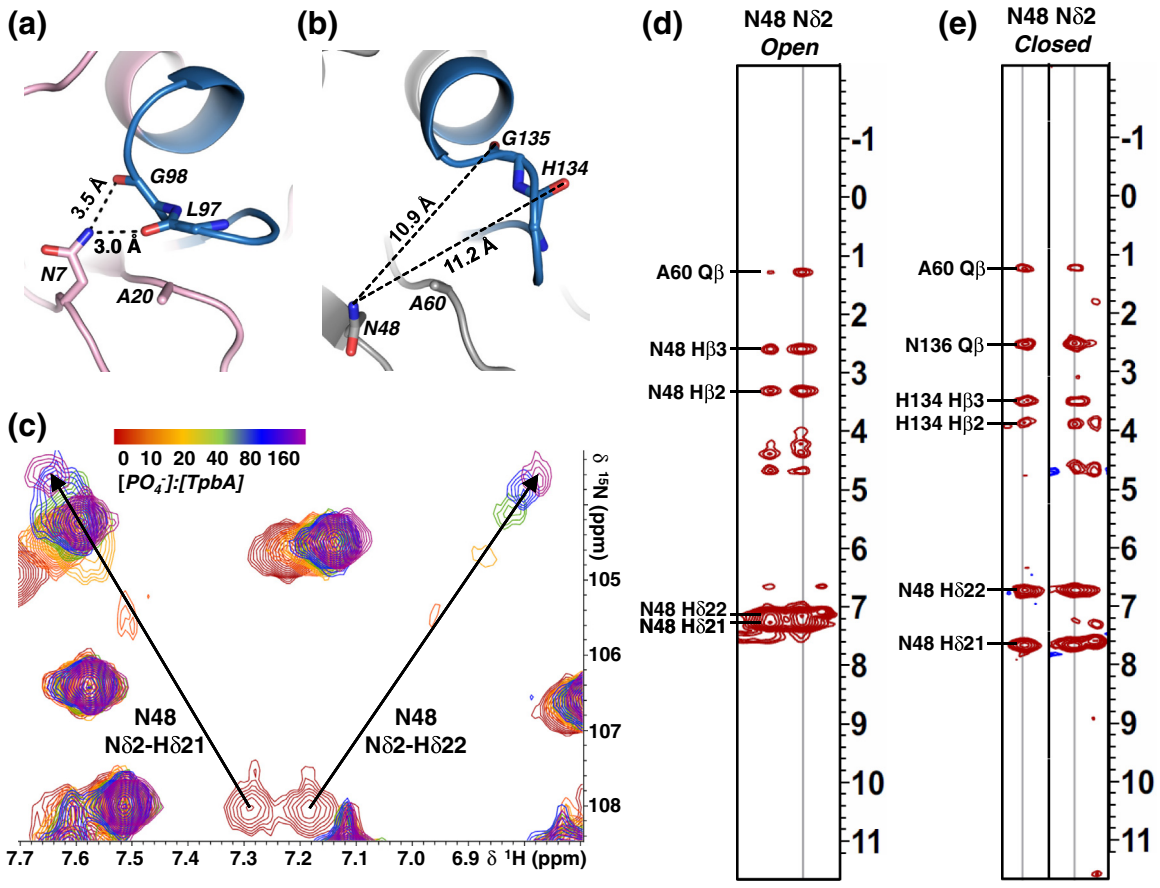

Fig. 4. Ligand binding causes structural changes in the PTP loop that involve N48. (a) The crystal structure of DUSP23 (PDB ID 2IMG) bound to malate (omitted for clarity). N7 makes polar contacts with the backbone carbonyls of PTP loop residues G98 and L97. Polar interactions are indicated by broken lines. (b) The lowest-energy structure of TpbA with residues homologous to those in (a) (N48, G135, and H134, respectively) is shown as sticks. The distances between N48 and the backbone carbonyls of G135 and H134 are shown as broken lines. (c) CSPs of the N48 side-chain protons, $H^{\delta21}$ and $H^{\delta22}$, in increasing concentrations of phosphate. (d) In the absence of substrate (*Open*), intra-residue NOEs are identified for N48 $H^{\delta21}$ and $H^{\delta22}$ side-chain protons. (e) Upon phosphate binding (*Closed*), NOEs to H134 and N136 are identified for N48 $H^{\delta21}$ and $H^{\delta22}$.

open and closed states of TpbA (Supplementary Figs. 5 and 6). The average R_1 relaxation rate of the core phosphatase domain (residues 40–194, including the PTP and general acid loops) changes between ligand-free open TpbA (1.15 ± 0.08 s^{-1}) and phosphate-bound closed TpbA (1.00 ± 0.09 s^{-1}), indicating a loss of nanosecond relaxation in closed TpbA. All of the core residues, for which the difference in R_1 between apo- and phosphate-bound states exceeds twice the propagated error in the measurements, have decreases in R_1, suggesting that this effect, though modest, is significant. Furthermore, the transverse relaxation rates for backbone ^{15}NH cross-peaks in the PTP motif and the general acid loop differ in the open and closed states. A plot of R_2/R_1 *versus* R_1R_2 highlights these differences[36] (Fig. 5). Residues in the PTP and general acid loops, namely, Asp105, Cys132, Gly135, and Thr139, are clear outliers in ligand-free TpbA, which is primarily attributed to elevated R_2 rates (Fig. 5a). The average R_2 value for these residues is 56.6 ± 7.2 s^{-1}, which is nearly twice that of the core phosphatase domain (29.6 ± 9.6 s^{-1}). This difference disappears in the phosphate-bound state (Fig. 5b) where the distribution of the ^{15}N relaxation states is tightly clustered in the R_2/R_1 *versus* R_1R_2 plot, with an average R_2 of 24.8 ± 4.0 s^{-1}. Again, while the R_2 averages show only a modest effect, in direct comparisons, 78% of core residues with significant differences in relaxation rates between apo- and bound states experienced a decline in R_2.

The reduced dynamic range for both R_2/R_1 and R_1R_2 indicates a loss of slower microsecond-to-millisecond motions associated with R_{ex}. This is consistent with the observation that exchange broadening impeded assignment of the backbone ^{15}NH pairs for many of these residues in the open conformation. For the same reason, quantitative relaxation measurements for His103 and Ala104 in the general acid loop, His134 and Asn136 in the PTP loop, Phe142 in helix α3, and Asp172 in the α4–α5 loop could not be obtained for ligand-free TpbA, but were readily measured in phosphate-bound TpbA (Supplementary Fig. 7). Upon titration of phosphate, these resonances sharpen significantly, indicating that they undergo a change in their dynamics from the intermediate-exchange to the fast-exchange regime. This is consistent with the overall decrease in R_1 for the PTP and general acid loops, supporting

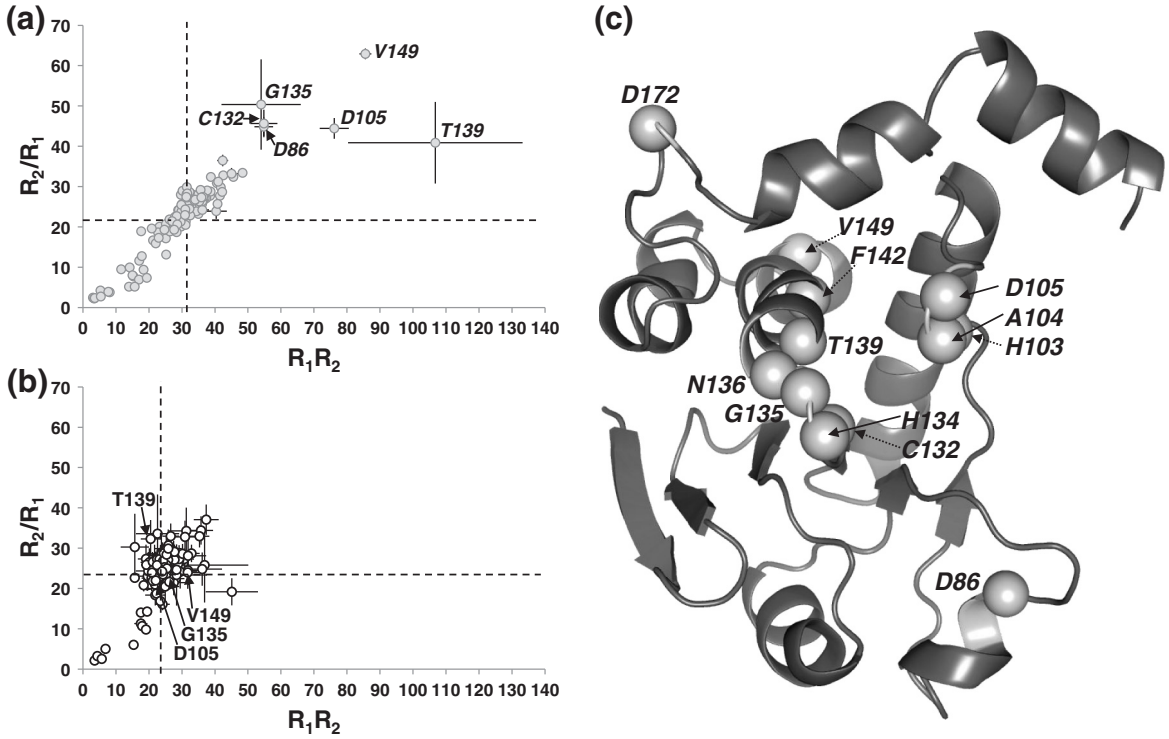

Fig. 5. The TpbA PTP and general acid loops experience a loss of microsecond/millisecond motions upon ligand binding. R_2/R_1 is plotted as a function of the product of R_1R_2 for (a) 1 mM ^{15}N-TpbA in the open conformation and (b) 0.97 mM ^{15}N-TpbA bound to phosphate (1:320 protein:ligand molar ratio) in the closed conformation. Error bars represent a propagation of errors from the relaxation measurements. Broken lines show the averages of R_2/R_1 and R_1R_2. (c) TpbA residues that experience a change in dynamics between the ligand-free and the phosphate-bound state are plotted as spheres on the lowest-energy structure of TpbA and labeled.

a loss of nanosecond motions in addition to the loss of microsecond-to-millisecond motions in these regions. These data, together with the sharply increased number of NOEs in phosphate-bound TpbA for many residues in the PTP, the general acid, and other active-site loops (Supplementary Fig. 4), strongly suggest that phosphate and/or ligand binding leads to a narrower range of conformational possibilities of the PTP and general acid loops in phosphate-bound TpbA (Fig. 5c).

Discussion

Our structure of TpbA is the first of a bacterial periplasmic DUSP and one of the few ligand-free open DUSPs. Equally important, our studies also provide the first detailed description of functionally important loop dynamics in a DUSP in the absence of ligand and show how they change in response to ligand binding. Taken together, this work significantly extends the small but growing body of evidence suggesting that cysteine-based phosphatases experience conformational flexibility in the open ligand-free state.[29–31,37,38] Furthermore, this is the first time that such an observation has been reported for a bacterial DUSP, showing that bacterial DUSPs may share not only structural but also dynamic similarities with their eukaryotic counterparts.

The catalytic activity and substrate specificity differ between DUSPs, depending on the enzyme itself and the substrate. For example, although the catalytic activity of the human DUSP VHZ against the nonspecific substrate *p*NPP is low (k_{cat} = 0.0094 s^{-1}),[39] it increases ~50-fold when the substrate is a phosphorylated peptide.[40] Similar to VHZ, we show that TpbA has a low catalytic activity against *p*NPP (k_{cat} = 0.00162 s^{-1}) and likely has a higher activity against a specific substrate. Presently, TpbB is the only known substrate of TpbA, and the primary amino acid sequence that is recognized by TpbA is currently unknown. Thus, identification of the TpbA-binding sequence in TpbB will be necessary to test TpbA catalytic activity against a specific substrate.

To date, only a small number of cysteine-based phosphatases have been characterized in the open state. This is because these proteins generally do not crystallize in the absence of ligand, and, because of their size, are also more difficult targets for structure determination using NMR spectroscopy. Moreover, even when open LMW-PTPs and DUSPs have been studied using NMR spectroscopy, NH cross-peaks for functionally relevant residues in the active loops are often missing. These observations suggest that these proteins are dynamic in the ligand-free open state, with the active-site loops likely adopting multiple conformations.[29–31,37,38] Here, we show that for TpbA, addition of the simplest ligand, inorganic phosphate, is sufficient to induce a significant change in both the structure and dynamics of its active-site loops, as evidenced by an increase of the number of NH cross-peaks in the ligand-bound 2D [^{1}H, ^{15}N] HSQC spectrum of TpbA. The phenomenon whereby ligand binding causes PTP loop resonances to appear in the NMR spectra has been observed in some phosphatases outside the DUSP family, such as LWM-PTPs.[30,37,38] However, the degree to which these active-site loops experience dynamics, and, furthermore, on which timescales, has not yet been reported. This is in part because these important regions are generally not detectable in the absence of ligand. Importantly, while many NH cross-peaks are weak in ligand-free TpbA, they can be detected. Thus, TpbA provides an unprecedented opportunity to further probe the nature of the dynamics that define the DUSP active site and, critically, to characterize how they change in response to ligand binding. Here, we report both fast (nanosecond) and slow (microsecond to millisecond) timescale dynamics for TpbA, the first time these motions have been examined in a DUSP. We discovered that ligand binding significantly changes the active-site loop dynamics. Our analysis shows that both fast- and intermediate-timescale dynamics change upon ligand binding, resulting in a narrower range of conformational possibilities for the PTP and general acid loops. That is, ligand binding reduces the conformational dynamics that occur on multiple timescales in the loops at the active site. Further investigation into the relationship between these dynamic motions in both phosphatase activity and substrate selectivity will facilitate the discovery of targeted inhibitors and activators, as well as further our understanding of the DUSP family.

Methods and Materials

Protein expression and purification

$TpbA_{29–218}$ was expressed in *E. coli* and purified as previously described.[12] $TpbA_{29–184}$, which lacks helix α6, was insolubly expressed in *E. coli*. Briefly, $TpbA_{29–218}$ was purified by Ni^{2+}-affinity chromatography and size-exclusion chromatography (Superdex 75 26/60) using 10 mM Tris–HCl, pH 7.8, 100 mM NaCl, and 0.5 mM TCEP as the final buffer. Partially ^{2}H, ^{15}N, ^{13}C-labeled $TpbA_{29–218}$ was expressed in *E. coli* cultures grown in M9 minimal media containing 4 g/L ^{13}C-D-glucose, 1 g/L ^{15}N-NH_4Cl, and 25% H_2O/75% D_2O. Cultures were grown at 37 °C and 250 rpm to a final OD_{600} of 0.9. Protein expression was induced with the addition of 1 mM IPTG and cultures were incubated for ~20 h (18 °C, 250 rpm). The protein yield was ~30 mg protein per liter of cell culture. Mass spectrometry (matrix-assisted laser desorption/ionization time of flight and electrospray ionization) was used to

determine the overall percentage of ^{2}H incorporation into the protein, which was ~45%.

NMR spectroscopy

NMR data were collected on Bruker Avance 500- and 800-MHz spectrometers equipped with TCI HCN *Z*-gradient cryoprobes at 298 K. NMR measurements of $TpbA_{29–218}$ were recorded using either ^{15}N- or $^{15}N,^{13}C$-labeled protein at a final concentration of 1 mM in 10 mM Tris, pH 7.8, 100 mM NaCl, 0.5 mM TCEP, and 90% H_2O/10% D_2O. Sequence-specific backbone and side-chain assignments were obtained as previously described.[12] Briefly, side-chain assignments for all aliphatic residues were obtained from a 3D HC(C)H-TOCSY (total correlated spectroscopy) spectrum (T_m = 12 ms, 800 MHz ^{1}H Larmor frequency), a 3D (H)CCH-TOCSY spectrum (T_m = 12 ms, 500 MHz ^{1}H Larmor frequency), and a 3D HC(C)H-COSY (correlated spectroscopy) spectrum (500 MHz ^{1}H Larmor frequency). NOE-based distance restraints were assigned from a 3D ^{15}N-resolved [$^{1}H,^{1}H$] NOESY (T_m = 65 ms, recorded at 800 MHz ^{1}H Larmor frequency), a 3D ^{13}C-resolved [$^{1}H,^{1}H$] NOESY (T_m = 65 ms, recorded at 800 MHz ^{1}H Larmor frequency), a 3D ^{13}C-resolved [$^{1}H,^{1}H$] NOESY (T_m = 65 ms, recorded at 800 MHz ^{1}H Larmor frequency; 45% ^{2}H/55% $^{1}H,^{15}N,^{13}C$-TpbA), and a 2D [$^{1}H,^{1}H$] NOESY (T_m = 65 ms, recorded at 800 MHz ^{1}H Larmor frequency; 100% D_2O solution). The ATNOS/CANDID software package[41,42] was used for automated NOESY peak picking and NOE assignment. Spectra were processed with Topspin 2.1/3.0/3.1 (Bruker, Billerica, MA) and data were evaluated using CARA†.

Structure calculation and refinement

A total of 2504 unambiguous NOESY-derived distance restraints along with 270 total dihedral angle restraints derived from ^{13}C-chemical shifts using TALOS+[43] were used in the initial structure calculations using CYANA.[41] Final energy-minimization and structure refinement was performed in explicit solvent using CNS 1.3[13] along with the RECOORD script package.[14] Two hundred structures were generated for each cycle and the 20 conformers with the lowest restraint violation energies were selected as the final representative model. The quality of the final ensemble of lowest-energy structures was assessed by the programs WHATCHECK,[44] AQUA,[45] and NMR-PROCHECK,[45] which are part of the iCing suite‡, and MOLMOL.[46] Ramachandran analysis showed that the TpbA structure has excellent stereochemistry with 98.4% of residues in the most favored and allowed region, 0.8% in the generously allowed region, and 0.8% in the disallowed region of the Ramachandran plot.

Phosphatase activity assay

Activity of TpbA against the general PTP/DUSP substrate, *p*-nitrophenyl phosphate (*p*NPP), was tested in 50 mM sodium acetate, pH 5.5, 100 mM NaCl, and 5 mM DTT. Forty microliters of enzyme at a 16-μM concentration was added to 60 μl of *p*NPP substrate resuspended in the reaction buffer. The final concentrations of *p*NPP used in this experiment were 0, 1, 2, 4, 8, and 16 mM. The enzyme was incubated with the substrate at 37 °C for 1 h, after which 100 μl of 1 M NaOH was added to a final concentration of 0.5 M NaOH to quench the reaction. Absorbance was measured at 405 nm and the final concentration of *p*-nitrophenol was calculated using the molar extinction coefficient of 18,000 M^{-1} cm^{-1}. A control reaction in which substrate was incubated in the absence of enzyme was subtracted from all other experimental values. All experiments were performed in triplicate and plotted as the average of the three experiments (error bars are the standard deviation). K_m and k_{cat} values were obtained by data fitting to the Michaelis–Menten model in Sigma Plot (Systat Software).

NMR analysis of phosphate binding

Sodium phosphate, pH 7.8, was titrated into 500 μM ^{15}N-TpbA at final concentrations of 5, 10, 20, 40, 80, and 160 mM, and 2D [$^{1}H,^{15}N$] HSQC spectra were recorded for each titration point. Chemical shift differences (Δδ) between ligand-free TpbA (0 mM phosphate) and phosphate-bound TpbA (160 mM phosphate) spectra were calculated using:

$$\Delta\delta(\text{ppm}) = \sqrt{(\Delta\delta_H)^2 + \left(\frac{\Delta\delta_N}{10}\right)^2}$$

The sequence-specific backbone assignment of phosphate-bound TpbA (1 mM $^{15}N,^{13}C$-TpbA, 320 mM sodium phosphate, 10 mM Tris, pH 7.8, 100 mM NaCl, and 0.5 mM TCEP) was achieved using the following experiments at 500 MHz ^{1}H Larmor frequency: 2D [$^{1}H,^{15}N$] HSQC, 3D HNCA, 3D HNCACB, 3D CBCA(CO)NH, and a 3D HBHA(CO)NH. A 3D ^{15}N-resolved [$^{1}H,^{1}H$] NOESY spectrum (T_m = 65 ms) was also recorded for phosphate-bound TpbA (1 mM ^{15}N-TpbA, 320 mM sodium phosphate, 10 mM Tris, pH 7.8, 100 mM NaCl, and 0.5 mM TCEP) at 800 MHz ^{1}H Larmor frequency.

Relaxation measurements and analysis

The same experiments were used to measure fast-timescale backbone dynamics for ligand-free TpbA (1 mM ^{15}N-TpbA, 10 mM Tris, pH 7.8, 100 mM NaCl, and 0.5 mM TCEP) and phosphate-bound TpbA (0.97 mM ^{15}N-TpbA, 310 mM sodium phosphate, 10 mM Tris, pH 7.8, 100 mM NaCl, and 0.5 mM TCEP; 1:320 molar ratio) at 500 MHz ^{1}H Larmor frequency. ^{15}N longitudinal (R_1) and transverse (R_2) relaxation rates and $^{15}N[^{1}H]$ NOE (hetNOE) measurements were acquired using sensitivity-enhanced experiments. T_1 and T_2 experiments were acquired with a recycle delay of 3 s between experiments, and the following relaxation delays for T_1: 5, 100, 400, 600, 800, 1000, 1200, and 1500 ms; and T_2: 17.36, 34.72, 69.44, 104.16, 121.52, 156.24, 173.6, 190.96, 208.32, and 243.04 ms. The total length of the T_2 relaxation delay is determined by the length of one Carr–Purcell–Meiboom–Gill cycle multiplied by the number of cycles (1–14 cycles). Systematic error in both T_1 and T_2 experiments was estimated from variance averaging of repetition experiments, which were acquired with delays of 100 and 800 ms for T_1 and 69.44 and 173.6 ms for T_2. The hetNOE measurements were determined from a pair of interleaved spectra acquired with

or without presaturation and a recycle delay of 5 s. R_1 and R_2 relaxation rates and the hetNOE were analyzed using Bruker Dynamics Center 2.0 (Bruker).

Accession numbers

All chemical shifts for ligand-free and phosphate-bound TpbA were deposited in the BioMagResBank[3] under accession numbers 18228 and 18977. Atomic coordinates for the ligand-free TpbA structure have been deposited in the Protein Data Bank (PDB) under the PDB code 2M3V.

Acknowledgements

The authors thank Drs. David A. Critton and Thusitha B. Jayasundera for help at early stages of the project, Dr. Joshua Wand (U. Penn) for helpful discussions, Dr. Torsten Herrmann (CNRS Lyon, France) for help with the structure calculation, and Dr. Tun-Li Shen (Brown University, Chemistry) for recording mass spectrometry data. This work was supported by NSF CAREER (MCB0952550 to R.P.) and the National Institutes of Health (GM089999 to T.K.W.). 800 MHz NMR data were recorded at Brandeis University (NIH S10-RR017269).

Supplementary Data

Supplementary data to this article can be found online at http://dx.doi.org/10.1016/j.jmb.2013.03.023

Received 5 February 2013;
Received in revised form 6 March 2013;
Accepted 13 March 2013
Available online 21 March 2013

Keywords:
dual-specificity phosphatase;
NMR spectroscopy;
open/closed state active-site dynamics;
bacterial signaling;
Pseudomonas aeruginosa

† http://cara.nmr.ch
‡ http://nmr.cmbi.ru.nl/cing/iCing.html

Abbreviations used:
TpbA, tyrosine phosphatase related to biofilm formation A; DUSP, dual-specificity phosphatase; PTP, protein tyrosine phosphatase; 2D, two-dimensional; 3D, three-dimensional; HSQC, heteronuclear single quantum coherence; NOE, nuclear Overhauser enhancement; NOESY, nuclear Overhauser enhancement spectroscopy; pTyr, phosphotyrosine; pSer, phosphoserine; pThr, phosphothreonine; WT, wild type; *p*NPP, *p*-nitrophenyl phosphate; CSP, chemical shift perturbation; PDB, Protein Data Bank.

References

1. Alonso, A., Sasin, J., Bottini, N., Friedberg, I., Osterman, A., Godzik, A. *et al.* (2004). Protein tyrosine phosphatases in the human genome. *Cell*, **117**, 699–711.
2. Diamond, R. H., Cressman, D. E., Laz, T. M., Abrams, C. S. & Taub, R. (1994). PRL-1, a unique nuclear protein tyrosine phosphatase, affects cell growth. *Mol. Cell. Biol.* **14**, 3752–3762.
3. Wu, J. J. & Bennett, A. M. (2005). Essential role for mitogen-activated protein (MAP) kinase phosphatase-1 in stress-responsive MAP kinase and cell survival signaling. *J. Biol. Chem.* **280**, 16461–16466.
4. Dickinson, R. J. & Keyse, S. M. (2006). Diverse physiological functions for dual-specificity MAP kinase phosphatases. *J. Cell Sci.* **119**, 4607–4615.
5. Reiterer, V., Grossniklaus, L., Tschon, T., Kasper, C. A., Sorg, I. & Arrieumerlou, C. (2011). Shigella flexneri type III secreted effector OspF reveals new crosstalks of proinflammatory signaling pathways during bacterial infection. *Cell. Signal.* **23**, 1188–1196.
6. Ueda, A. & Wood, T. K. (2009). Connecting quorum sensing, c-di-GMP, pel polysaccharide, and biofilm formation in *Pseudomonas aeruginosa* through tyrosine phosphatase TpbA (PA3885). *PLoS Pathog.* **5**, e1000483.
7. Hassett, D. J., Sutton, M. D., Schurr, M. J., Herr, A. B., Caldwell, C. C. & Matu, J. O. (2009). *Pseudomonas aeruginosa* hypoxic or anaerobic biofilm infections within cystic fibrosis airways. *Trends Microbiol.* **17**, 130–138.
8. Costerton, W., Veeh, R., Shirtliff, M., Pasmore, M., Post, C. & Ehrlich, G. (2003). The application of biofilm science to the study and control of chronic bacterial infections. *J. Clin. Invest.* **112**, 1466–1477.
9. Pu, M. & Wood, T. K. (2010). Tyrosine phosphatase TpbA controls rugose colony formation in *Pseudomonas aeruginosa* by dephosphorylating diguanylate cyclase TpbB. *Biochem. Biophys. Res. Commun.* **402**, 351–355.
10. Denu, J. M. & Dixon, J. E. (1995). A catalytic mechanism for the dual-specific phosphatases. *Proc. Natl Acad. Sci. USA*, **92**, 5910–5914.
11. Barford, D., Das, A. K. & Egloff, M. P. (1998). The structure and mechanism of protein phosphatases: insights into catalysis and regulation. *Annu. Rev. Biophys. Biomol. Struct.* **27**, 133–164.
12. Koveal, D., Jayasundera, T. B., Wood, T. K., Peti, W. & Page, R. (2013). Backbone and sidechain (1)H, (15)N and (13)C assignments of tyrosine phosphatase related to biofilm formation A (TpbA) of *Pseudomonas aeruginosa*. *Biomol. NMR Assign.* **7**, 57–59.
13. Brunger, A. T., Adams, P. D., Clore, G. M., DeLano, W. L., Gros, P., Grosse-Kunstleve, R. W. *et al.* (1998). Crystallography & NMR system: a new software suite for macromolecular structure determination. *Acta Crystallogr., Sect. D: Biol. Crystallogr.* **54**, 905–921.
14. Nederveen, A. J., Doreleijers, J. F., Vranken, W., Miller, Z., Spronk, C. A., Nabuurs, S. B. *et al.* (2005). RECOORD: a recalculated coordinate database of 500+ proteins from the PDB using restraints from the BioMagResBank. *Proteins*, **59**, 662–672.

15. Gruninger, R. J., Selinger, L. B. & Mosimann, S. C. (2009). Structural analysis of a multifunctional, tandemly repeated inositol polyphosphatase. *J. Mol. Biol.* **392**, 75–86.
16. Chu, H. M., Guo, R. T., Lin, T. W., Chou, C. C., Shr, H. L., Lai, H. L. *et al.* (2004). Structures of *Selenomonas ruminantium* phytase in complex with persulfated phytate: DSP phytase fold and mechanism for sequential substrate hydrolysis. *Structure*, **12**, 2015–2024.
17. Puhl, A. A., Gruninger, R. J., Greiner, R., Janzen, T. W., Mosimann, S. C. & Selinger, L. B. (2007). Kinetic and structural analysis of a bacterial protein tyrosine phosphatase-like myo-inositol polyphosphatase. *Protein Sci.* **16**, 1368–1378.
18. Myers, M. P., Pass, I., Batty, I. H., Van der Kaay, J., Stolarov, J. P., Hemmings, B. A. *et al.* (1998). The lipid phosphatase activity of PTEN is critical for its tumor supressor function. *Proc. Natl Acad. Sci. USA*, **95**, 13513–13518.
19. Slack, D. N., Seternes, O. M., Gabrielsen, M. & Keyse, S. M. (2001). Distinct binding determinants for ERK2/p38alpha and JNK map kinases mediate catalytic activation and substrate selectivity of map kinase phosphatase-1. *J. Biol. Chem.* **276**, 16491–16500.
20. Xie, L., Zhang, Y. L. & Zhang, Z. Y. (2002). Design and characterization of an improved protein tyrosine phosphatase substrate-trapping mutant. *Biochemistry*, **41**, 4032–4039.
21. Flint, A. J., Tiganis, T., Barford, D. & Tonks, N. K. (1997). Development of "substrate-trapping" mutants to identify physiological substrates of protein tyrosine phosphatases. *Proc. Natl Acad. Sci. USA*, **94**, 1680–1685.
22. Stewart, A. E., Dowd, S., Keyse, S. M. & McDonald, N. Q. (1999). Crystal structure of the MAPK phosphatase Pyst1 catalytic domain and implications for regulated activation. *Nat. Struct. Biol.* **6**, 174–181.
23. Kozlov, G., Cheng, J., Ziomek, E., Banville, D., Gehring, K. & Ekiel, I. (2004). Structural insights into molecular function of the metastasis-associated phosphatase PRL-3. *J. Biol. Chem.* **279**, 11882–11889.
24. Roma-Mateo, C., Rios, P., Tabernero, L., Attwood, T. K. & Pulido, R. (2007). A novel phosphatase family, structurally related to dual-specificity phosphatases, that displays unique amino acid sequence and substrate specificity. *J. Mol. Biol.* **374**, 899–909.
25. Agarwal, R., Burley, S. K. & Swaminathan, S. (2008). Structure of human dual specificity protein phosphatase 23, VHZ, enzyme-substrate/product complex. *J. Biol. Chem.* **283**, 8946–8953.
26. Gray, C. H., Good, V. M., Tonks, N. K. & Barford, D. (2003). The structure of the cell cycle protein Cdc14 reveals a proline-directed protein phosphatase. *EMBO J.* **22**, 3524–3535.
27. Vander Kooi, C. W., Taylor, A. O., Pace, R. M., Meekins, D. A., Guo, H. F., Kim, Y. & Gentry, M. S. (2010). Structural basis for the glucan phosphatase activity of Starch Excess4. *Proc. Natl Acad. Sci. USA*, **107**, 15379–15384.
28. Alonso, A., Rojas, A., Godzik, A. & Mustelin, T. (2003). The dual-specific protein tyrosine phosphatase family. *Topics in Current Genetics,* pp. 5, Springer, Berlin.
29. Kim, K. A., Song, J. S., Jee, J., Sheen, M. R., Lee, C., Lee, T. G. *et al.* (2004). Structure of human PRL-3, the phosphatase associated with cancer metastasis. *FEBS Lett.* **565**, 181–187.
30. Hu, J., Li, D., Su, X. D., Jin, C. & Xia, B. (2010). Solution structure and conformational heterogeneity of acylphosphatase from *Bacillus subtilis*. *FEBS Lett.* **584**, 2852–2856.
31. Farooq, A., Plotnikova, O., Chaturvedi, G., Yan, S., Zeng, L., Zhang, Q. & Zhou, M. M. (2003). Solution structure of the MAPK phosphatase PAC-1 catalytic domain. Insights into substrate-induced enzymatic activation of MKP. *Structure*, **11**, 155–164.
32. Stehle, T., Sreeramulu, S., Lohr, F., Richter, C., Saxena, K., Jonker, H. R. & Schwalbe, H. (2012). The apo-structure of the low molecular weight protein-tyrosine phosphatase A (MptpA) from *Mycobacterium tuberculosis* allows for better target-specific drug development. *J. Biol. Chem.* **287**, 34569–34582.
33. Kim, S. J., Jeong, D. G., Yoon, T. S., Son, J. H., Cho, S. K., Ryu, S. E. & Kim, J. H. (2007). Crystal structure of human TMDP, a testis-specific dual specificity protein phosphatase: implications for substrate specificity. *Proteins*, **66**, 239–245.
34. Jeong, D. G., Yoon, T. S., Kim, J. H., Shim, M. Y., Jung, S. K., Son, J. H. *et al.* (2006). Crystal structure of the catalytic domain of human MAP kinase phosphatase 5: structural insight into constitutively active phosphatase. *J. Mol. Biol.* **360**, 946–955.
35. Yuvaniyama, J., Denu, J. M., Dixon, J. E. & Saper, M. A. (1996). Crystal structure of the dual specificity protein phosphatase VHR. *Science*, **272**, 1328–1331.
36. Kneller, J. M., Lu, M. & Bracken, C. (2002). An effective method for the discrimination of motional anisotropy and chemical exchange. *J. Am. Chem. Soc.* **124**, 1852–1853.
37. Gustafson, C. L., Stauffacher, C. V., Hallenga, K. & Van Etten, R. L. (2005). Solution structure of the low-molecular-weight protein tyrosine phosphatase from *Tritrichomonas foetus* reveals a flexible phosphate binding loop. *Protein Sci.* **14**, 2515–2525.
38. Logan, T. M., Zhou, M. M., Nettesheim, D. G., Meadows, R. P., Van Etten, R. L. & Fesik, S. W. (1994). Solution structure of a low molecular weight protein tyrosine phosphatase. *Biochemistry*, **33**, 11087–11096.
39. Alonso, A., Burkhalter, S., Sasin, J., Tautz, L., Bogetz, J., Huynh, H. *et al.* (2004). The minimal essential core of a cysteine-based protein-tyrosine phosphatase revealed by a novel 16-kDa VH1-like phosphatase, VHZ. *J. Biol. Chem.* **279**, 35768–35774.
40. Kuznetsov, V. I., Hengge, A. C. & Johnson, S. J. (2012). New aspects of the phosphatase VHZ revealed by a high-resolution structure with vanadate and substrate screening. *Biochemistry*, **51**, 9869–9879.
41. Guntert, P. (2004). Automated NMR structure calculation with CYANA. *Methods Mol. Biol.* **278**, 353–378.
42. Herrmann, T., Guntert, P. & Wuthrich, K. (2002). Protein NMR structure determination with automated NOE-identification in the NOESY spectra using the new software ATNOS. *J. Biomol. NMR*, **24**, 171–189.
43. Shen, Y., Delaglio, F., Cornilescu, G. & Bax, A. (2009). TALOS+: a hybrid method for predicting protein

backbone torsion angles from NMR chemical shifts. *J. Biomol. NMR*, **44**, 213–223.
44. Hooft, R. W., Vriend, G., Sander, C. & Abola, E. E. (1996). Errors in protein structures. *Nature*, **381**, 272.
45. Laskowski, R. A., Rullmannn, J. A., MacArthur, M. W., Kaptein, R. & Thornton, J. M. (1996). AQUA and PROCHECK-NMR: programs for checking the quality of protein structures solved by NMR. *J. Biomol. NMR*, **8**, 477–486.
46. Koradi, R., Billeter, M. & Wuthrich, K. (1996). MOLMOL: a program for display and analysis of macromolecular structures. *J. Mol. Graphics*, **14**, 29–32.